Salem et al. Integrating Materials and Manufacturing Innovation 2014, 3:24
http://www.immijournal.com/content/3/1/24

Integrating Materials and Manufacturing Innovation
a SpringerOpen Journal

REVIEW Open Access

Workflow for integrating mesoscale heterogeneities in materials structure with process simulation of titanium alloys

Ayman A Salem[1*], Joshua B Shaffer[1], Daniel P Satko[1], S Lee Semiatin[2] and Surya R Kalidindi[3]

* Correspondence:
ayman.salem@icmrl.net
[1]Materials Resources LLC, Dayton, OH 45402, USA
Full list of author information is available at the end of the article

Abstract

In this paper, a generalized workflow is outlined for the necessary integration of multimodal measurements and multiphysics models at multiple hierarchical length scales demanded by an Integrated Computational Materials Engineering (ICME) approach to accelerated materials development. Recognizing that multiple choices or techniques are typically available in each of the main steps, several exemplary analyses are detailed utilizing mainly the alpha/beta titanium alloys as an illustrative case. It is anticipated that the use and further refinement of these workflows will promote transparency and engender intimate collaborations between materials experts and manufacturing/design specialists by providing an understanding of the various mesoscale heterogeneities that develop naturally in the workpiece as a direct consequence of the inherent heterogeneity imposed by the manufacturing history (i.e., different thermomechanical histories at different locations in the sample). More specifically, this article focuses on three main areas: (i) data science protocols for efficient analysis of large microstructure datasets (e.g., cluster analysis), (ii) protocols for extracting reduced descriptions of salient microstructure features for insertion into simulations (e.g., regions of homogeneity), and (iii) protocols for direct and efficient linking of materials models/databases into process/performance simulation codes (e.g., crystal plasticity finite element method).

Keywords: ICME; Microstructure informatics; Higher-order statistics; Materials big data; Macrozones; Region of homogeneity; Representative orientation distribution; Alpha/beta titanium alloys

Review

Introduction

Predicting mechanical response and texture evolution during thermomechanical processing (TMP) of alpha/beta titanium alloys is challenging due to the complexity of the underlying microstructure in the alloys and the highly anisotropic response exhibited by the microscale constituents. Not only do these materials exhibit two phases with drastically different deformation mechanisms, but also the morphology, crystallography, and relative ratio of the phases changes with temperature and deformation path. Consequently, there have been many research efforts focusing on various sources of anisotropy in these materials [1,2]. With the recent push of the Materials Genome Initiative (MGI) and Integrated Computational Materials Engineering (ICME) towards

a coherent integration between various stages and scales of modeling the materials behavior and the corresponding measurements, new workflows (i.e., protocols) are critically needed. In this article, an example workflow is presented that integrates materials characterization (both microstructure and mechanical response) with suitable multiscale simulations of processing conditions (Figure 1). This workflow comprises the following general operations: (i) assembly of information gathered about the local state of the materials from experimental or modeling data into a feature vector; (ii) application of data analytics techniques to identify particular features of interest; (iii) creation of representative descriptors of microstructure features that provide an optimized reduced description; and (iv) insertion of the representative descriptors into materials models that evolve the microstructure and properties during TMP, making use of a particular solver architecture (e.g., finite element method (FEM)) with various degrees of feedback. The path of the workflow can also be closed through post-processing operations whereby the results of materials models are used to update the local state information, enriching the information contained in the feature vector.

In order to provide for a greater understanding of the various operations and the flow of information throughout the workflow, detailed descriptions of exemplary illustrations are provided in the subsequent sections. In particular, discussion is focused on examples illustrating how a series of choices can be made to advance the incorporation of titanium microstructures into numerical simulations of a part production. The workflow and selected techniques are directed towards the emerging 'Big-Data' materials innovation ecosystem that utilizes modern data science techniques such as machine learning and computer vision [3,4]. While the Ti-6Al-4V microstructure data presented here were generated with standard

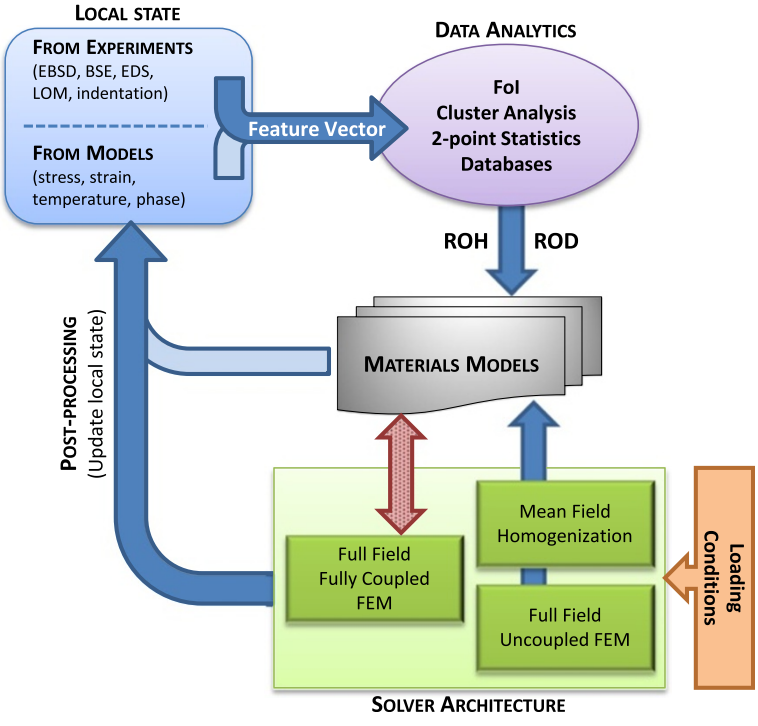

Figure 1 A Big-Data based ICME workflow. A generic workflow is given for integrating mesoscale heterogeneities in material structure with process simulation of titanium alloys.

methods (e.g., electron backscatter diffraction (EBSD) and backscattered electron (BSE) imaging), they were recorded from large scan areas resulting in 100,000,000s of EBSD data points and 10,000s of high-resolution BSE images. Consequently, new tools have had to be developed for texture analysis, image segmentation, and quantification of microstructure metrics. In addition, salient microstructure descriptors (e.g., regions of homogeneity (ROH), representative orientation distributions (ROD), and microtextured regions or macrozones (MTR)) have been generated using a new generation of data analytics techniques.

Microstructure of α-β titanium alloys

Due to the strong effect of microstructure on the mechanical behavior of materials, it is important to have a clear understanding of the various constituents of the microstructure and their influence on the mechanical behavior and texture evolution under a broad range of loading conditions. Ti-6Al-4V was selected as the primary model material in the following sections to describe our workflow. This alloy exhibits a dual-phase microstructure with a hexagonal close-packed (HCP) alpha phase and a body-centered cubic (BCC) beta phase that coexist in various volume fractions based on the temperature history of the sample or component. Thermomechanical processing of this alloy produces a range of microstructures that can be categorized into three major types: fully lamellar, fully equiaxed, and bimodal (Figure 2). For the same chemistry, the volume fractions, morphology, and texture of the constituents are known to have a major effect on the mechanical behavior of the alloy [5].

Lamellar and equiaxed microstructures have constituents with distinct morphologies that can be extracted using standard image segmentation techniques applied on BSE or optical images. Consequently, extracting alpha laths in the lamellar microstructure or alpha particles (not grains) in the equiaxed microstructure (Figure 2a,b) can be done using contrast thresholding in a commercial software package (e.g., ImageJ and Photoshop) due to the image contrast resulting from etching (optical) or atomic number difference (BSE) of the two phases. However, the bimodal microstructure is a challenge because the alpha phase has two morphological constituents, namely, primary alpha particles and secondary alpha colonies with alternating alpha laths and beta layers (Figure 2c). Because both constituents have the same HCP crystal structure, regular EBSD maps cannot automatically distinguish between them (Figure 3a). The same challenge lies while using the BSE images (Figure 2c) alone. On smaller areas, the use of multimodal signals and traditional thresholding techniques has succeeded to segment (α_p) particles and (α_s) colonies based

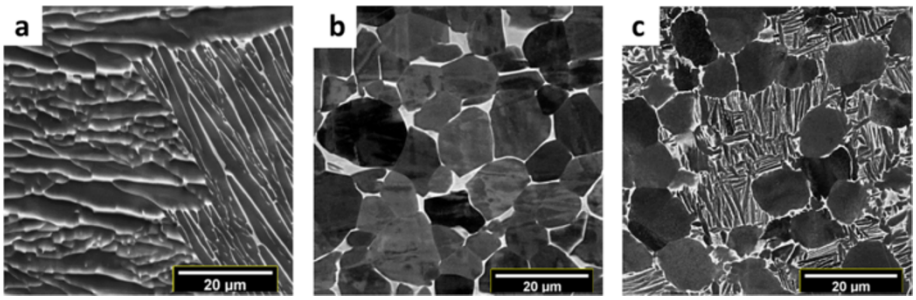

Figure 2 Common microstructures in α-β titanium alloys. Backscatter electron (BSE) images of **(a)** fully lamellar microstructure, **(b)** fully equiaxed microstructure, and **(c)** bi-modal microstructure.

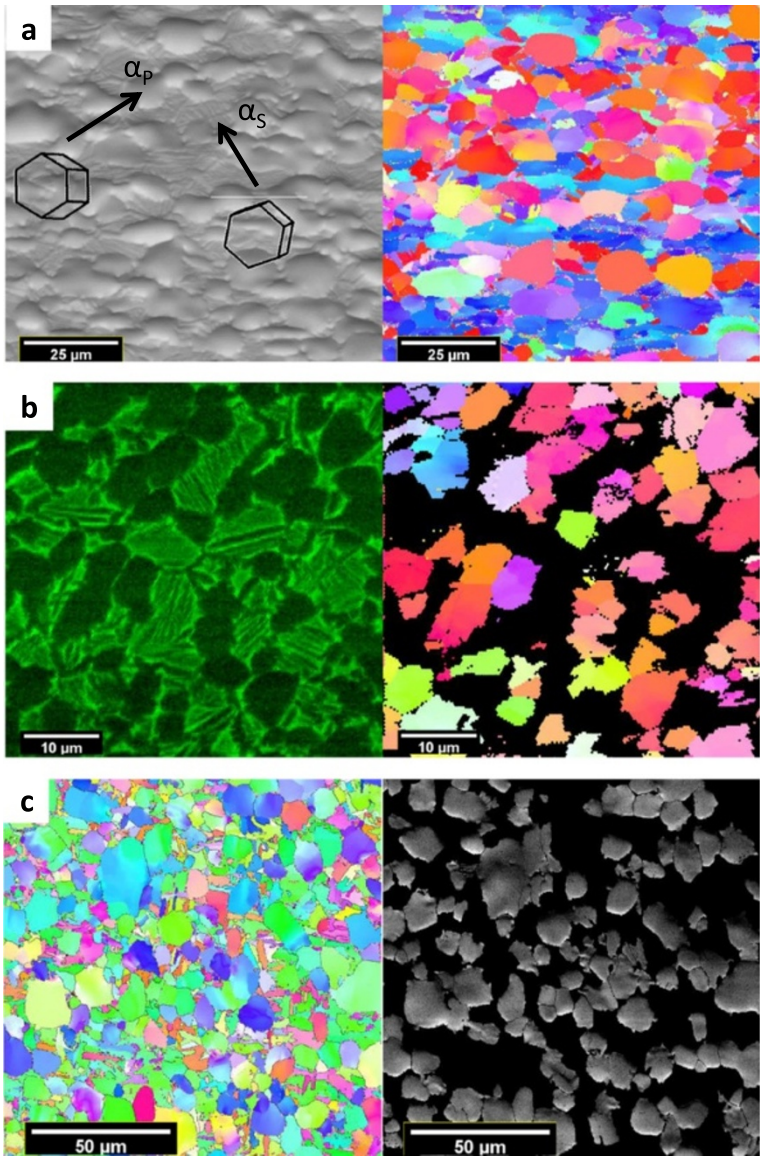

Figure 3 Segmenting HCP constituents (α_p and α_s) in Ti-6Al-4V. (a) Secondary electron image of a bimodal Ti-6Al-4V alloy with primary particles (α_p) and secondary alpha colonies (α_s) and ND-IPF map of Ti-6Al-4V with indistinguishable HCP constituents (α_p grains and α_s colonies). **(b)** Using a map of vanadium concentration generated by EDS showing higher concentration in secondary alpha (α_s) colonies to segment the α_p particles. **(c)** Alpha-phase inverse pole figure map and resultant EBSD pattern quality map of auto-segmented α_p grains using TiSeg™.

on vanadium partitioning (Figure 3b) [6]. However, applying these methods to large areas for practical applications is expensive and time-consuming. The use of data science approaches (as described in detail in subsequent sections) has enabled automated segmentation of 10,000s of EBSD and BSE datasets (Figure 3c).

Data analytics for large microstructure datasets

The bimodal microstructure contains many microstructure features (α_p particles, α_p grains, α_s colonies, α_s laths, layers of alpha on beta grain boundaries, prior β grains, microtextured

regions, etc.) that can affect the response of the material under loading. However, the data captured by typical characterization techniques (EBSD, BSE, spectroscopy, etc.) do not directly identify these microstructure features automatically. Rather, at each probed location, the data include signals from the materials that reflect the internal local state of the materials. These internal variables change with time under externally applied variables (e.g., temperature, cooling rate, strain). As such, one can assign the local state at each voxel location in the studied area using a list of internal variables that are related to the crystal structure and alloying elements of the underlying materials. The microstructure features mentioned earlier are then defined by certain morphological characteristics displayed by the local states. Consequently, it should be possible to use various cluster analysis techniques [7] to identify the features of interest (FoI) from large datasets (e.g., EBSD scan of 10×10 mm at 1 μm step size giving 10^8 measurements of the local state). An example is the familiar spatial clustering of measurement points sharing a common orientation that is understood as a 'grain'. Similarly, the spatial clustering of a group of grains indicates a microtextured region (macrozone), while the spatial clustering of similar chemical elements is indicative of micro/macrosegregation or precipitates. As such, taking advantage of recent advances [8] in data science has enabled the development of multiple algorithms and tools for quantifying the microstructural features of interest in computationally efficient ways [9]. In the next few sections, the main terminologies and methodologies used in these workflows are introduced.

Feature vector

Each voxel in a materials dataset is assigned an n-dimensional feature vector [10] of variables needed to obtain a concise mathematical representation of all the distinct local states in the dataset. Such representation facilitates image processing, statistical analysis, and utilization of numerous algorithms from the pattern recognition and machine learning communities [11] to extract salient information about the material. The list of variables used in the feature vectors can range from scalar variables (e.g., chemical composition) to tensorial variables (e.g., crystal lattice orientation). These feature vectors play an important role in identifying proper materials models for process simulations (e.g., thermomechanical processing of Ti alloys).

While the main goal of materials Big-Data efforts is to improve the accuracy of predictive modeling, the implementation of such efforts is often faced with the doubt that 'bigger is not always better' [12]. This unfortunate stigma has surfaced in fields other than materials science where low signal-to-noise ratio is the norm [13] and the main question often is exactly what data needs to be collected. Furthermore, the high cost of collecting materials data often results in the production of very sparse datasets relative to the high degree of heterogeneity possible in large manufactured structures. Similar challenges have faced predictive modeling of human behavior, though the large economic gains that have been realized from the success of these models have in turn helped to improve the popularity and the accuracy of such efforts [12,13]. Recently, Fortuny et al. [12] provided empirical support that predictive performance from sparse fine-grained (behavior) data was increased by using Big-Data. For example, using KDD Cup 2010 student evaluation data, Fortuny et al. [12] showed that the predictive power (area under receiver operating characteristic, ROC) for the multinomial Naïve Bayes

variants increased with the addition of more data (Figure 4). Such correlation is likely also applicable to predictive modeling with materials Big-Data with an expected improvement in accuracy of predictions due to the absence of noise inherent in the often emotion-driven behavior of human populations.

Identification of features of interest

As noted earlier, the local states do not necessarily identify the microstructure features of interest directly, necessitating additional analysis. As such, prior knowledge in the field will help identify the specific microstructural FoI (presumably these features control the performance characteristics of the final finished product) that need to be tracked in the process simulations. Automated protocols for the extraction of selected features of interest are needed to obtain consistency and reproducibility independent of operator bias and with minimum computational cost. Due to the importance of the FoI as the main building block for further analysis and modeling efforts, computer vision algorithms built on supervised and unsupervised machine learning techniques [11] should be employed for automated feature identification and extraction.

To extract specific FoI, some or all components of a feature vector can be used in the cluster analysis [7]. For example, for identifying only the beta phase, a single variable in the feature vector (e.g., BCC phase in EBSD dataset) is adequate. However, segmenting primary alpha grains in bimodal microstructures requires clustering data regarding orientation, chemistry, and/or imaging contrast at each voxel in the microstructure dataset. Distinguishing between primary alpha grains and primary alpha particles is important for accurate predictions of materials responses that depend on the slip distance (e.g., crystal plasticity). An α_p particle (Figure 5a) may engulf multiple α_p grains (Figure 5b), though in the case of a microstructure that has been fully spherodized during the ingot breakdown process, a particle may include only one grain. As such, while identification of particles can be accomplished directly from BSE images (Figure 2c) by finding the remnant beta

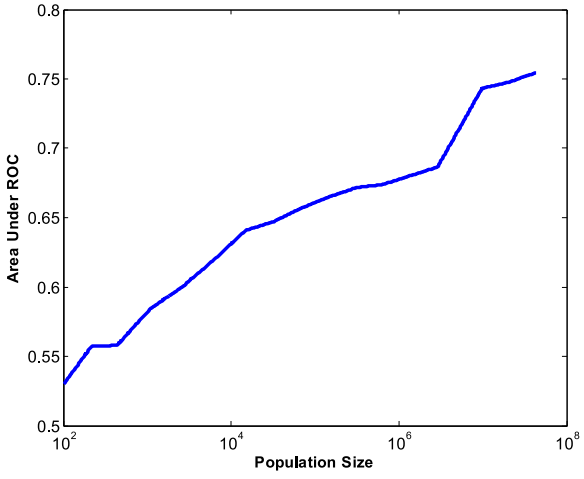

Figure 4 Learning curves with increasing numbers of features. Adding more data (x-axis) leads to continued improvement of the predictive power (area under ROC). Dataset from KDD Cup 2010: student performance evaluation [12].

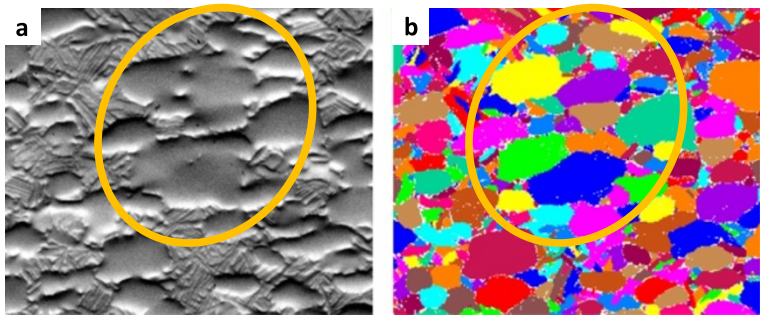

Figure 5 Distinguishing between particles and grains in Ti-6Al-4V. (a) Secondary electron image with primary alpha particles shown as continuous islands in a sea of secondary alpha laths and **(b)** EBSD data of the same location with individual primary alpha grains colored differently. Almost all primary alpha particles in **(a)** contain multiple primary alpha grains as shown in **(b)** with an example highlighted in the circle.

layer separating particles, further differentiation of α_p grains within a particle requires orientation information in addition to BSE information (Figure 3c, Figure 5b).

Independent of the length scale, a feature of interest may be defined as *a region in physical space (3D) that depicts similar characteristic feature vectors as some other regions in the microstructure*. This definition enables setting up automated extraction tools that are mainly dependent on the components of the feature vector. In the case mentioned above, the feature vector for alpha 'particle' identification needs only one element (BSE gray level), while a larger feature vector is necessary to define primary alpha 'grains' (BSE gray level + orientation). To achieve automation and to increase the speed of extraction, the identification is conducted in a two-step process in two separate domains. The first step is conducted in the feature vector domain (i.e., feature space) in which volumes with similar feature vectors are classified using cluster analysis [7]. The second step is conducted in physical space by mapping the classified clusters from the first step to corresponding spatial locations in real space. To demonstrate the FoI concept practically on Ti-6Al-4V, EBSD, and BSE data within a feature vector are used to extract information about MTRs which can be defined as 3D regions in physical space that contain similarly oriented primary alpha grains [14].

Prior attempts to identify MTRs were based on traditional EBSD data analysis methods available in commercial EBSD data analysis tools [15]. However, these methods do not scale well for large datasets ($>10^7$ EBSD data points covering hundreds of square millimeters and $>10^5$ BSE images). However, the two-step process [14] described above has enabled the rapid identification of MTR clusters, each distributed about a common texture component with a defined misorientation range (<10° in this case) within each cluster. The cluster analysis was conducted with a feature vector of 551 dimensions in domain of the generalized spherical harmonics (GSH), a mathematical construct commonly used to analytically describe the distribution of crystallographic orientations [16-21]. The normal direction (ND) inverse pole figure (IPF) maps in Figure 6a, b show the variability of the length scale from primary alpha grains in (b) to MTRs in (a). One of the identified MTR cluster families is shown in real space in Figure 6c, along with the corresponding GSH-space projection (Figure 6d), demonstrating the orientation clustering of various MTR families.

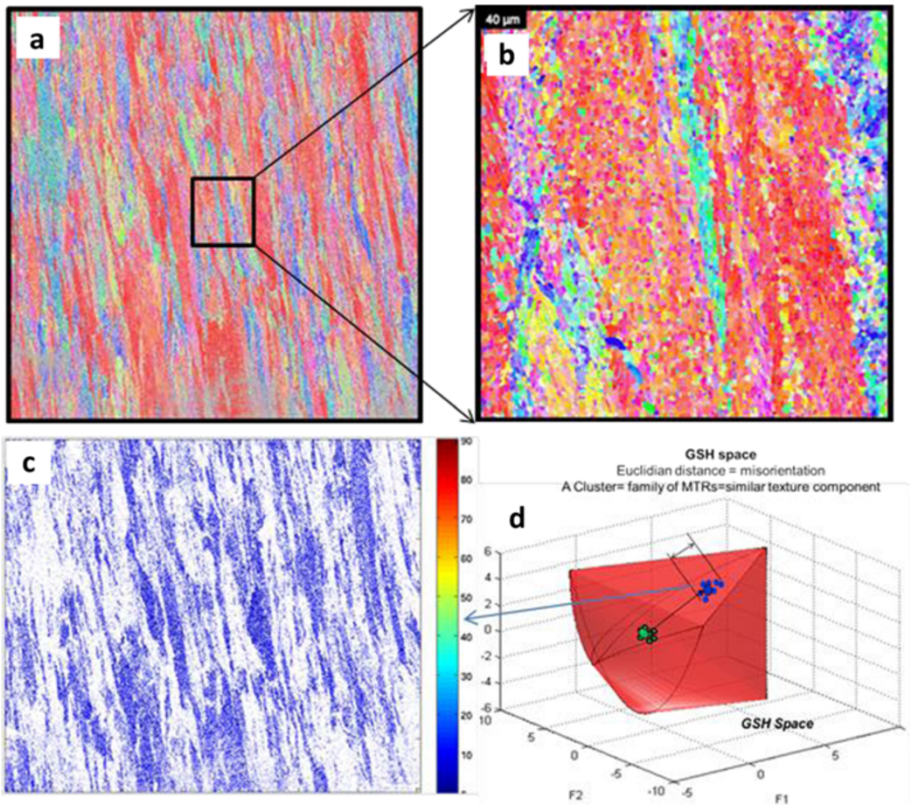

Figure 6 Identifying features of interest at multiple length scales. (a) ND-IPF from EBSD scan of 8.8 × 8.8 mm Ti-6Al-4V plate at 2.5 μm step size. **(b)** Enlargement of the central region of the scan showing details of individual primary alpha grains. **(c)** Real-space mapping of the MTR blue family with the color reflecting the misorientation between a pixel and the MTR centroid orientation. **(d)** Visualization of GSH space with the blue MTR cluster as recognized by unsupervised machine learning. Note that the mean class variance was less than 8°.

Representative descriptions of microstructure

Regions of homogeneity

Identifying specific subsets that represent the whole material has been the target of many research efforts including finding a representative volume element (RVE) [22,23] and/or the statistical volume element (SVE) [24]. One of the defining features of an RVE or SVE description is the linking of materials properties of the ensemble to the properties of the defined RVE or SVE. For example, Drugan and Willis [23] defined an RVE as 'a smallest material volume element of the composite for which the usual spatially constant "overall modulus" macroscopic constitutive representation is a sufficiently accurate model to represent mean constitutive response'. However, estimating the materials response depends on the defined RVE/SVE, so defining the RVE or SVE that is based on the response of the material to use it in models that predict the response of the material becomes a challenging task. Furthermore, many of the traditional methods used to define RVEs/SVEs are based on highly simplified metrics (e.g., average grain size and its distribution) and ignore the spatial correlations of individual FoI (e.g., complex morphologies that may not fit a standard geometrical shape such as an ellipse). While the traditional methods may work for materials with homogeneous spatial distributions of the FoI, it may not be efficient for heterogeneous spatial distributions of FoI such as MTRs (Figure 6c) or gradient microstructures. In both cases, there is a need for

microstructure representation that captures the essence of spatial and morphological heterogeneities. Presented below is a new microstructure descriptor (regions of homogeneity) that has been developed based on the spatial homogeneity of the two-point statistics that were calculated for sampled microstructure regions.

The hierarchical materials systems described here exhibit salient features at different length scales. For example, in the Ti alloys described here, one scale of heterogeneity occurs at the length scale of individual α_p grains (on the order of 10 to 30 μm) and another scale of heterogeneity occurs at the scale of each MTR (up to several mm in length). In multiscale modeling, one typically identifies different length scales where one might be able to homogenize the materials response by aggregating in some way all of the inherent heterogeneity below that length scale. In materials with complex structures, one has to identify suitable hierarchical length scales for homogenization, which are called regions of homogeneity. ROH can be established objectively at different hierarchical length scales by carefully quantifying spatial correlations (e.g., using two-point spatial correlations [17,25-30]) and finding suitable window sizes in the microstructure that capture the inherent heterogeneity (FoI and their spatial distributions) to a desired accuracy. It is also desired to keep these ROH small enough to enable cost-effective modeling (the computational cost rises steeply with increases in the number of voxels needed to capture the ROH).

For example, the dataset in Figure 6 was iteratively divided into 12 subsets with 12 different window sizes. Each subset consisted of multiple fixed size windows resulting in a total of 2,912 windows. For each subset, the two-point correlations were calculated for the microstructure inside each window. Then, the difference between the median of the two-point correlations of each subset and the whole dataset was measured via a Euclidean distance (D) and plotted in Figure 7 as a function of window size within each subset. The two-point correlation of the median for subset with window size of 2.2 × 2.2 mm was the closest to the two-point statistics of the original larger dataset (smallest distance D in Figure 7). Consequently, the median of windows with size of 2.2 × 2.2 mm can represent the microstructure details regarding the features of interest (i.e., MTRs) including size, morphology, and spatial distributions for dataset in Figure 6.

It is worth noting that in the above example, the FoI (specifically MTRs) were large relative to the scanned area. As such, a window size smaller than 2.2 × 2.2 mm did not

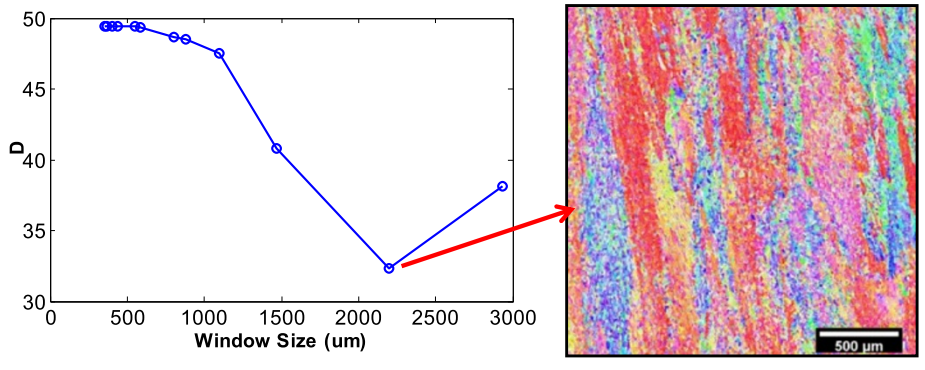

Figure 7 Comparison of two-point statistics of windows and ensemble to determine ROH size. The distance between the median of the two-point statistics of ensemble of windows and the whole dataset. The horizontal axis is the size of windows in each ensemble, giving a 2.2 × 2.2 mm ROH of the two-point statistics.

provide an adequate representation of the microstructure in the original scanned area. However, the same technique to find ROH can be applied to FoI with a size much smaller than the scanned area. For example, individual primary alpha particles in a Ti-6Al-4V plate hot rolled at 955°C [31] have a typical size of about 12 μm, covering an area of <0.05% relative to total area of the captured image (490 × 745 μm, Figure 8a). Following the method developed by Niezgoda et al. [28], the selection of ROH is demonstrated using weighted two-point statistics of subsets of the microstructure. Niezgoda et al. [28] showed that an RVE generated with this method can result in minimum deviation in the effective modulus compared to the original microstructure modulus. Similar results have also been presented by Qidwai et al. [32] and Wargo et al. [33] in very different application domains. Here, the same technique is applied without a reference to the material properties, and to distinguish between both approaches, the ROH approach is used to reflect the weighted representative microstructure without calculating any

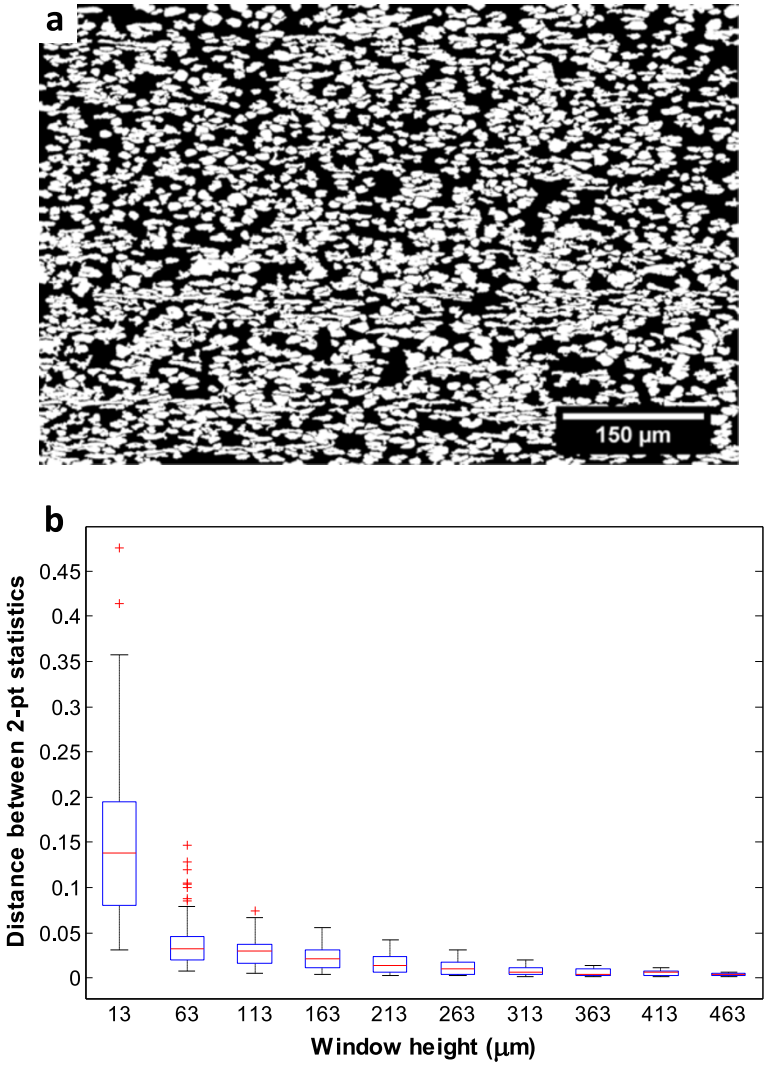

Figure 8 Variation of two-point statistics with respect to window size. (a) Segmented BSE image showing primary alpha particles in Ti-6Al-4V after hot rolling at 955°C and **(b)** Euclidean measure (D) of the distance between two-point statistics of microstructures as a function of window sizes. Each box gives an average distance and the distribution of the distances between microstructures in the given ensemble.

associated properties. For the microstructure in Figure 8a, 100 windows were sampled from the image and the median and variance within each sample were quantitatively measured in the two-point statistics domain in which the differences can be measured via a Euclidean distance (D) in Figure 8b.

A window size of 247 × 163 μm was observed to show saturation in the mean separation (D) of the two-point statistics within an ensemble. A comparison of the two-point statistics of one of these selected windows and the statistics of the full window (Figure 9a,b) shows a close similarity in the short-range order, with only minor differences at longer range. The example window and its position relative to the total image are shown in Figure 9c,d, respectively. The inclusion of additional weighted windows results in a smaller error between the ensemble statistics and the ROH from the weighted windows providing a trade-off between increased accuracy of the ROH description and computational cost. Window selection is accomplished by nonnegative least squares regression after decomposition of the two-point statistics via principal component analysis (PCA; Figure 10a) [8]. The weighted combination of the three windows given in Figure 10b gives the ROH with the smallest error in PCA space (Figure 11a) compared to the total image (Figure 11b, also shown in red in Figure 10a).

The next step after generating the two-point correlations of the ROH is to generate the microstructure in the ROH to be used in materials models. This inverse reconstruction process is meant to create statistically similar microstructures that account for morphological and spatial heterogeneities that were captured within the ROH [30,34,35]. The process of reconstruction from the two-point correlation has been proven accurate for

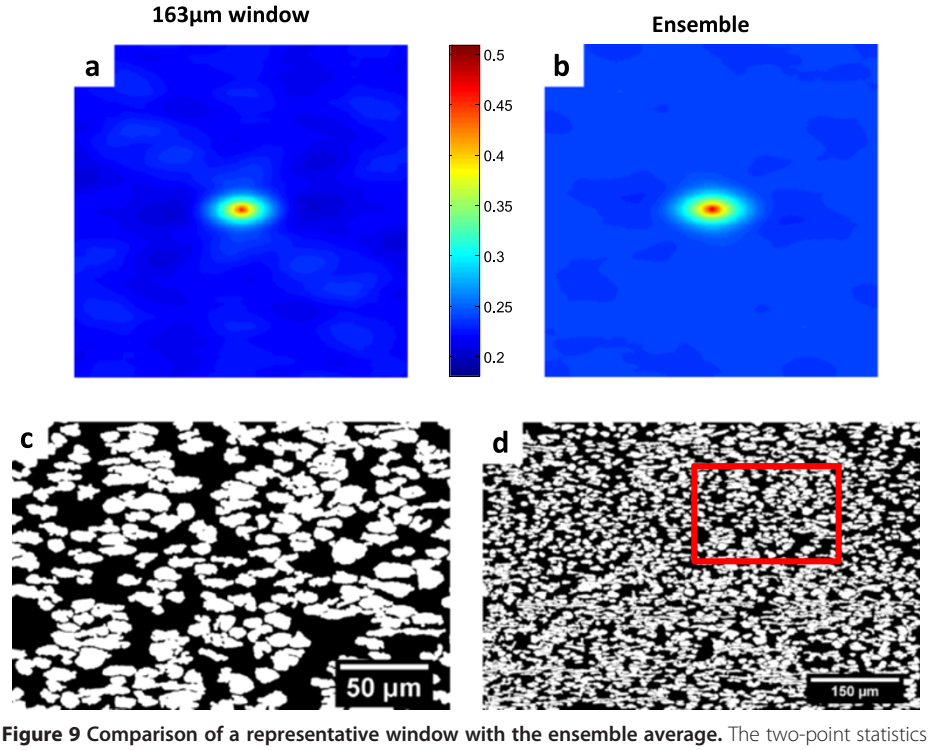

Figure 9 Comparison of a representative window with the ensemble average. The two-point statistics of **(a)** a 163 × 247 μm window and **(b)** the entire dataset. The segmented microstructure **(c)** corresponding to the window in **(a)** and (**d**) its location within the whole microstructure.

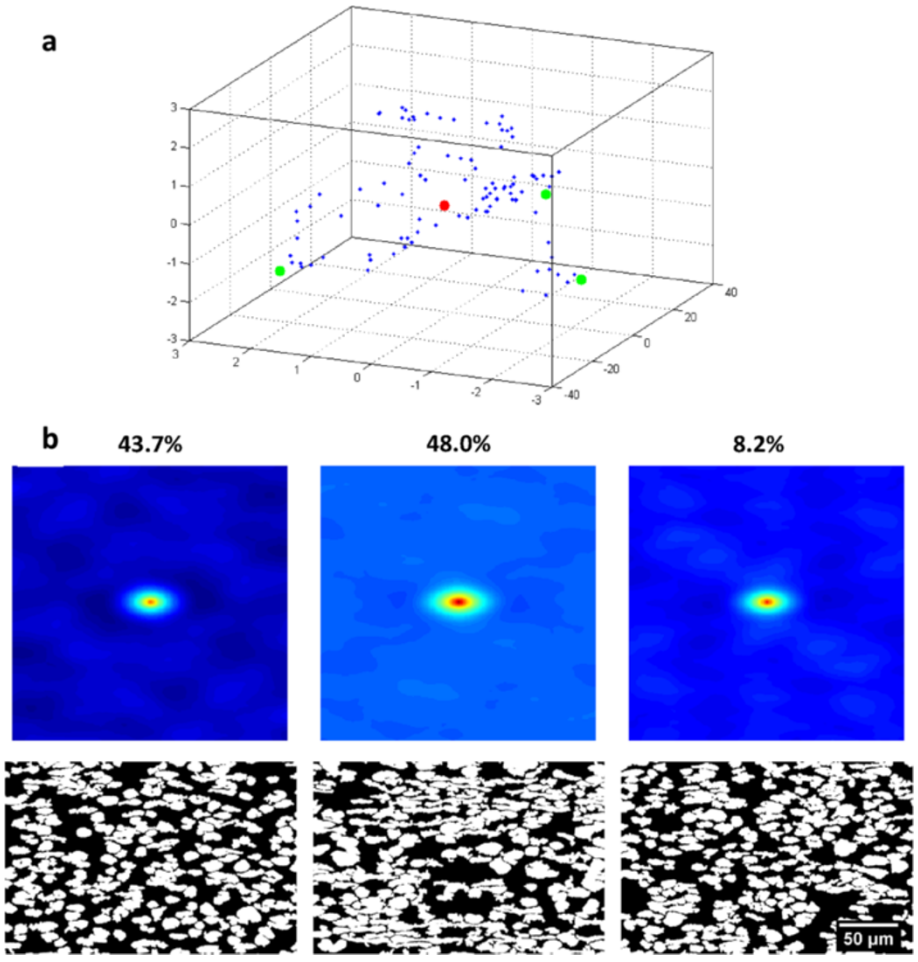

Figure 10 Selection of three weighted windows to achieve minimum deviation of the ROH from ensemble average. (a) Visualization of the first three principal components for the two-point statistics of 163 × 247 μm windows, with each point representing a window. The location of the ensemble is given in red. The weighted sum of the three windows highlighted in green achieves the minimum deviation from the ensemble. **(b)** Microstructures and associated two-point statistics for three weighted windows.

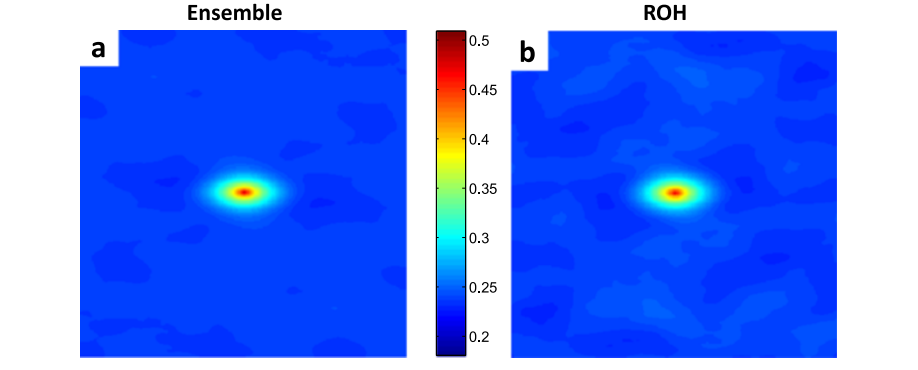

Figure 11 Using a weighted average from several windows to improve ROH accuracy. (a) Two-point statistics of the entire dataset (Figure 8a) and **(b)** ROH from weighted two-point statistics of three windows in Figure 9.

images with two phases within an inversion and translation of the original image, while prescribing periodic boundary conditions (Figure 12) [30].

Representative orientation distribution

The exceedingly large number of crystallographic orientations recorded during data collection for MTR identification represents a challenge for predicting texture evolution using any crystal plasticity model. Consequently, it is crucial to develop a procedure that finds a representative orientation distribution consisting of a reduced number of orientations giving the same texture as the measured large dataset. Recently, in an example case study, it has been demonstrated that a set of weighted 551 orientations is able to reproduce exactly (with an error of 10^{-17} in the orientation distribution function (ODF)) the same texture as the 12,467,961 (Figure 13) orientations measured in the Ti-6Al-4V sample given in Figure 6. To give an estimate of the time savings, a Taylor-type crystal plasticity modeling of simple compression to strain of −1.0 was executed in 1.6 mins on a standard desktop computer (quad-core 3.0 GHz) using the ROD. Under an approximation of linear time complexity with the number of orientations evolved, the identical simulation is estimated to take more than 25 days to run with the original dataset on the same computer.

Materials models: crystal plasticity

Titanium exhibits highly anisotropic properties at the single-crystal level, which can be attributed to the operation of different deformation mechanisms under different external stimuli (temperature, strain rate, etc.). In addition to the numerous competing deformation mechanisms [36], there also exist additional challenges due to the fact that an allotropic transformation occurs from alpha-HCP to beta-BCC at high temperatures (beta transus is dependent on alloying elements). The addition of alloying elements causes the alpha and beta phases to coexist with varying ratios and morphologies based on the temperature and the amount of alpha or beta stabilizers. This consequently alters the activity of various deformation mechanisms depending on the resultant microstructure. For example, the Ti-6Al-4V with bimodal microstructure shown previously (Figure 2) accommodates plastic deformation through slip in both alpha and beta phases, with the latter contribution increasing as the deformation temperature increases. As such, accurate

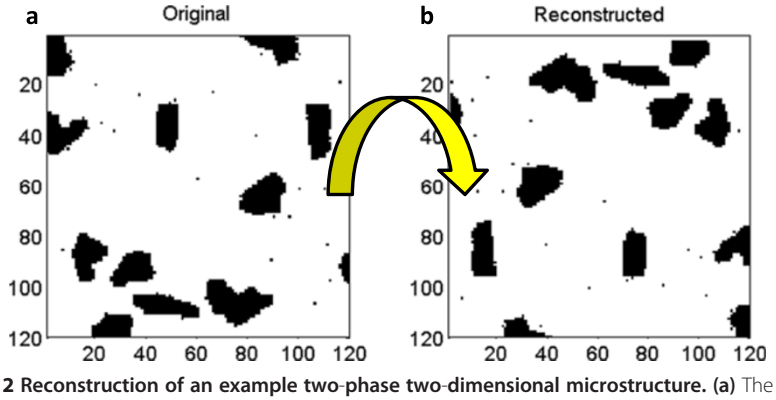

Figure 12 Reconstruction of an example two-phase two-dimensional microstructure. (a) The original microstructure and **(b)** the reconstructed microstructure which matches the original within an inversion as indicated by the arrow.

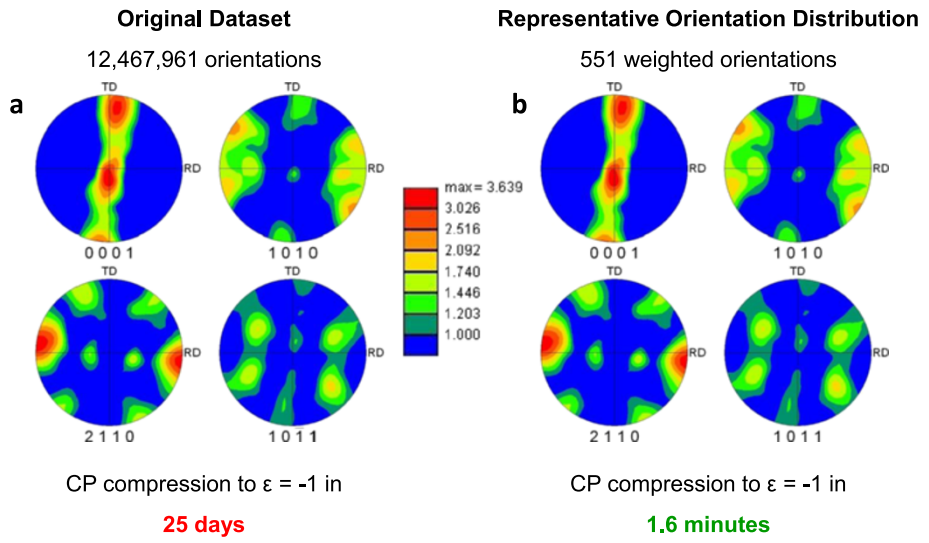

Figure 13 Using ROD as a compact representation of large orientation datasets. (a) Pole figure calculated from the EBSD dataset of sample in Figure 6 with approximately 12.5 million orientations and **(b)** the texture calculated from ROD with only 551.

modeling of the mechanical behavior and texture evolution of this material requires an understanding on the crystal level of the various deformation mechanisms of each phase, the interaction between both phases, and their evolution as a function of temperature.

Single-crystal deformation behavior

Deformation mechanisms in the alpha phase (HCP) of unalloyed titanium and the two-phase materials are limited to a finite number of slip systems and/or deformation twinning which results in pronounced anisotropic behavior and strong deformation texture [36]. In particular, deformation can be accommodated by prism < a > and basal < a > slip which result in only four independent slip systems [36]. Hence, extension or contraction of the HCP c-axis requires activation of pyramidal < c + a > slip and/or deformation twinning, both of which exhibit high resistance to activation. The activity of any slip or twin system occurs once the resolved shear stress exceeds the critical resolved shear stress (CRSS) on that system. The values of the CRSS can be calibrated using experimental stress-strain data [37,38]. Once these values are estimated for the materials under a selected deformation path, the validated values can be subsequently used to predict the mechanical behavior and texture evolution under any applied deformation using crystal plasticity modeling [39].

On the other hand, the beta phase (BCC) is known to accommodate plastic deformation exclusively by slip on various reported slip systems. Some simulations have used pencil glide on any slip plane containing <111 > slip systems [40,41]. Others have assumed slip on {110}, {112}, and {123} planes [42,43]. The abovementioned options should be available in any practical crystal plasticity model.

In two-phase Ti-6Al-4V with a colony microstructure, the alpha and beta phases are known to maintain a Burgers orientation relationship [44], creating an easy pathway for dislocation transmission across the interface for aligned slip systems, with resistance increasing with increased misalignment [45]. Consequently, the presence of such interfaces

and limitations imposed by slip transmission across the interface results in anisotropy within individual slip systems. For example, compression experiments conducted on large single-colony samples demonstrated a significant difference between yield and hardening on the prism $< a_1 >$ and prism $< a_3 >$ slip systems (Figure 14) [45].

A single crystal under external applied strain deforms from a reference configuration to a deformed configuration, with this change being described by a deformation gradient tensor, **F**. To separate elastic and plastic deformations, Kröner [46] suggested the multiplicative decomposition of the deformation gradient into elastic ($\mathbf{F}^{*}$) and plastic ($\mathbf{F}^{p}$) components (Figure 15). The plastic component $\mathbf{F}^{p}$ causes the permanent deformation of the materials, and it is applied in an intermediate configuration which maintains a perfect lattice. As such, estimating how a single crystal accommodates plastic deformation by crystallographic slip or twinning (pseudo slip [47]) can be conducted in the intermediate configuration using the starting orientation of the single crystal [37]. Further details of the crystal plasticity theory are presented in Figure 15 and have been explained elsewhere [39].

Polycrystalline deformation behavior

Most metallic parts are made of polycrystalline and/or multiphase alloys which require homogenization methods to predict their response starting with the single-crystal constitutive equations. Furthermore, calibrating single-crystal CRSSs and its evolutions (strain hardening) require comparisons with experimental measurements which are mostly conducted on polycrystalline materials.

In addition to homogenization methods, strain partitioning between coexisting phases is also used to capture the overall mechanical response and texture evolution of two phase materials (e.g., Ti-6Al-4V) [48].

Homogenization method: Taylor approach

To relate the deformation of an aggregate to the deformation of a single crystal, homogenization (i.e., mean field) methods have been used based on iso-strain, iso-

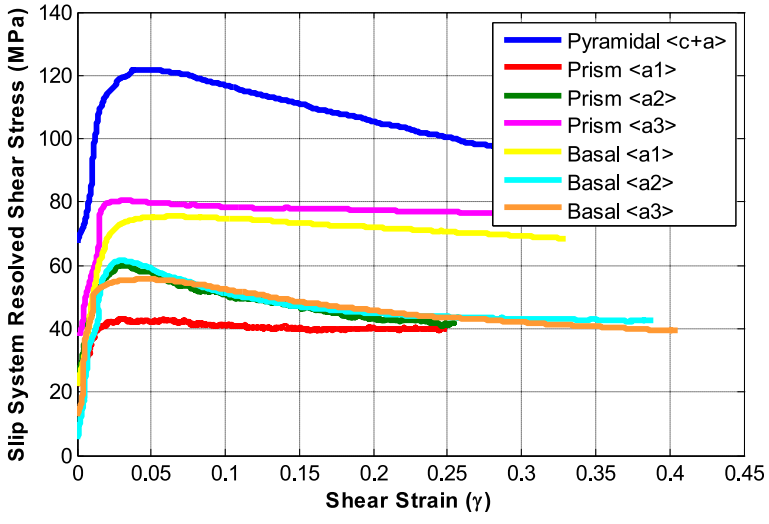

Figure 14 Single colony Ti-6Al-4V stress-strain data. Samples were sectioned from large single colonies to facilitate the activity of a single slip system under simple compression testing at 815°C.

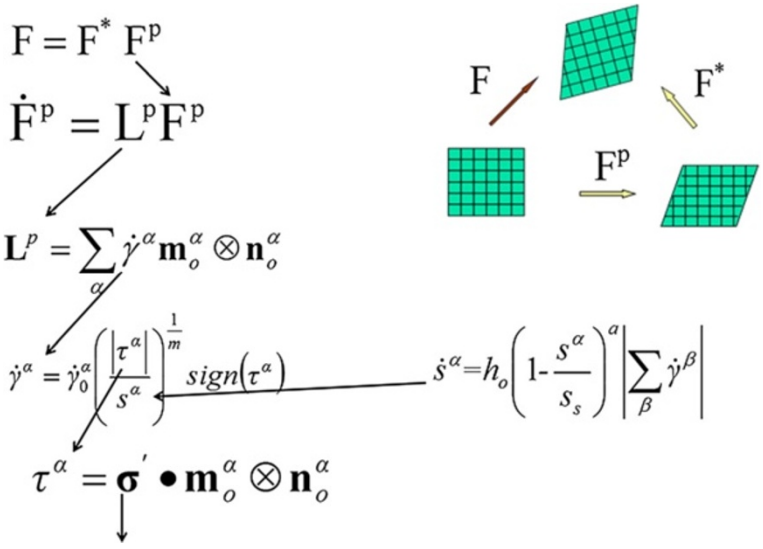

Figure 15 Calculating the slip system resolved shear stress. The plastic deformation gradient is used in the intermediate configuration after the multiplicative decomposition to calculate the resolved shear stress τ^α on the slip system α.

stress, or viscoplastic self-consistent assumptions [49]. The simplest approach is the iso-strain approach based on Taylor's model [50], which assumes that the deformation gradient experienced by individual crystallites is equal to the applied deformation gradient for the aggregate. While the method violates stress compatibility, it has been popularly applied as an upper-bound technique and has been used in simulating texture evolution of the beta phase during hot working breakdown operations above the beta transus temperature for production-scale ingots of Ti-6Al-4V [42] and during hot rolling in the beta field [51], with deformation accommodated by slip. At room temperatures, the alpha phase deforms by a combination of slip and twinning which was successfully simulated (Figure 16) using the Taylor assumption in both high purity Ti [37] and commercial purity Ti [52]. Due to the wide use of the Taylor approach, attention is focused in subsequent

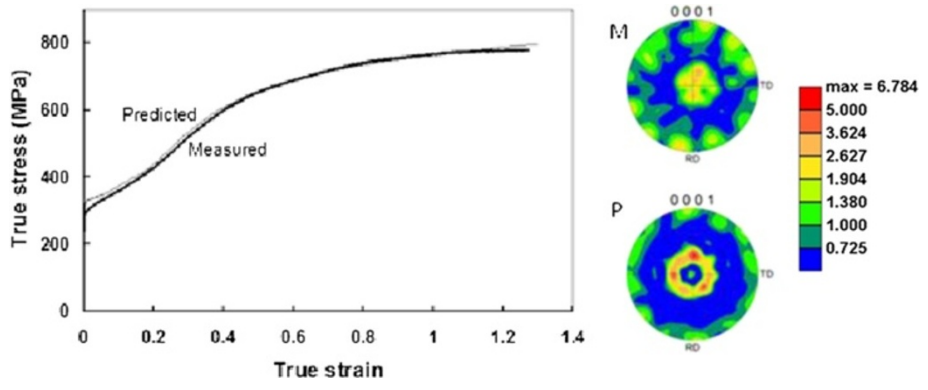

Figure 16 Crystal plasticity modeling of titanium involving combined slip and twinning. Taylor-type crystal plasticity model predictions of room temperature simple compression in pure Ti showing stress-strain curves and 0001 pole figures after true strain of −0.56.

sections on this method and to examining various methods to increase the speed of integration into FEM codes.

Spectral crystal plasticity

The use of Taylor-type models requires repeating the single-crystal calculations for each orientation within the input texture. However, when simulating real parts with varying textures at different locations in the part (as identified by the ROH), traditional Taylor calculations take a very long time to execute, and full-field simulations, such as crystal plasticity finite element method (CPFEM) (described in more detail below), can require several orders of magnitude more computational time. However, the use of spectral crystal plasticity based on fast Fourier transforms (FFTs) [53,54] has resulted in major time savings (Figure 17). The use of discrete Fourier transform (DFT) databases enables efficient calculations using spectral crystal plasticity [55]. In particular, this database is constructed for all possible orientations under all possible deformation gradients. The building of such a database constitutes a onetime effort investment. Consequently, subsequent computations of crystal plasticity are carried out by using the database. Figure 17 shows about 45× increase in the speed of calculations for interstitial-free (IF) steel (BCC) [56]. Similar databases for HCP are under development.

Full-field crystal plasticity finite element simulations

In the previously discussed Taylor-type approach, the local deformation gradient is assumed to be the same as the global deformation gradient an assumption that needs to be relaxed for most commercially used alloys with complex dual-phase microstructures. Finite element methods offer a practical solution to calculating the grain-scale heterogeneity present in the deformation field. Consequently, crystal plasticity models have been coupled with commercial finite element codes to explore highly sophisticated homogenization schemes. Some commercial FEM codes enable the implementation of crystal plasticity materials constitutive behavior as a user-subroutine (e.g., UMAT/

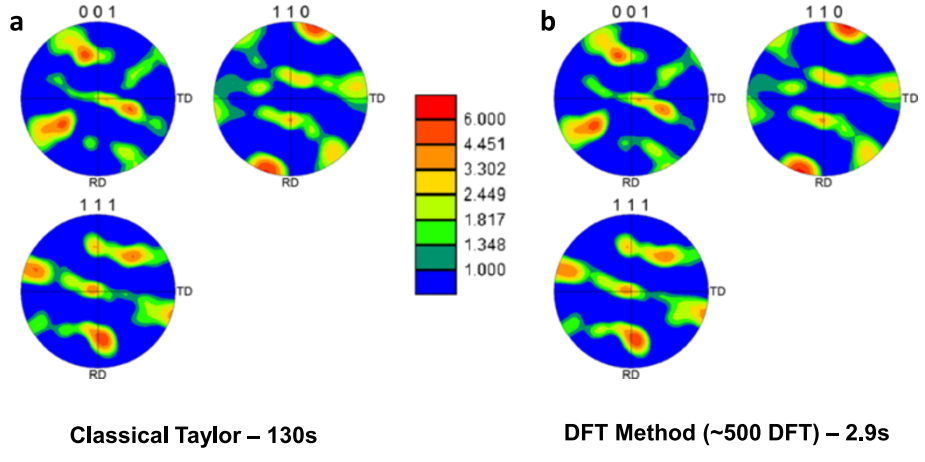

Figure 17 Increasing the speed of crystal plasticity modeling using DFT. Compared to classical methods **(a)**, the spectral crystal plasticity method **(b)** showed a drastic decrease in computational time for prediction of texture in polycrystalline IF steel (BCC) under simple shear ($\gamma = 0.6$). All calculations were conducted on a Pentium 4 desktop PC [56].

VUMAT in ABAQUS [57] and Hypela2 in Marc [58] and Simufact [59]. For implicit codes, the crystal plasticity user-subroutine is expected to (1) calculate the stress based on the imposed local deformation history and (2) calculate the local Jacobian matrix (defined as $d\Delta\sigma/d\Delta\varepsilon$). As such, once the appropriate user subroutine is verified to work for a crystal structure, further validation and calibration can be done by users for various materials within the same crystal structure. Adopting this method results in full-field simulations, also known as CPFEM simulations. While they provide higher accuracy in predicting the materials behavior, they are known to be slow for large simulations. The use of spectral crystal plasticity [60] has demonstrated an improvement of the calculation speed more than 30× compared to the conventional approaches (Figure 18). Further increase in the speed of calculation can be achieved by using the ROH and the ROD concepts described above.

In certain situations, it becomes necessary to simulate multiscale coupled phenomena at two well-separated length scales. As an example, consider the simulation of a complex processing operation where different macroscale spatial locations in the workpiece experience different thermomechanical histories (often an unavoidable consequence of the boundary conditions imposed at the macroscale). Consequently, strong variations in the microstructure should be expected at different locations in the workpiece. In other words, it is not enough to track the evolution of a single representative microstructure for the entire workpiece. The development of such microstructure heterogeneities can be expected to influence the macroscale simulation by altering the local effective properties at different locations in the workpiece. In such a situation, it is necessary to track independently microstructures at multiple macroscale locations in the workpiece and pass high value information in both directions (between the microscale and the macroscale). This is extremely difficult, if not impossible, using any of the currently employed computational strategies.

The challenge described above can be addressed with modest computational resources using a data science approach called materials knowledge systems (MKS) [61-66]. In the MKS framework, the focus is on localization (i.e., opposite of homogenization) relationships that capture the spatial distribution of the response field of interest (e.g., stress or

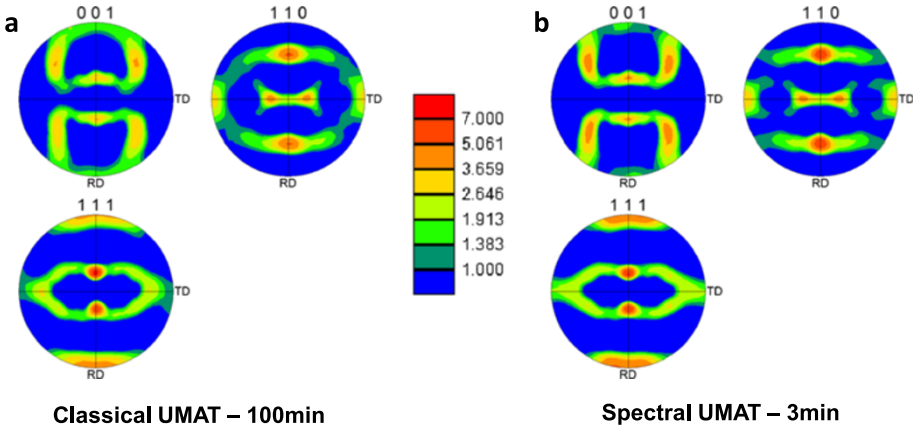

Figure 18 Application of spectral methods to coupled CPFEM. An increase in calculation speed of almost two orders of magnitude is verified by incorporating spectral crystal plasticity as a user subroutine with FEM code ABAQUS vs. a comparable integrated classical user subroutine for copper. **(a)** Classical UMAT and **(b)** spectral UMAT [60].

strain rate fields) at the microscale (on an RVE) for an imposed loading condition at the macroscale. In this approach, the localization relationships are expressed as calibrated metamodels that take the form of a simple algebraic series whose terms capture the individual contributions from a hierarchy of local microstructure descriptors. Each term in this series expansion is expressed as a convolution of the appropriate local microstructure descriptor and its corresponding influence at the microscale. The series expansion in the MKS framework is in complete accord with the series expansion obtained in the physics-based statistical continuum theories [30,67-70]. The MKS approach dramatically improves the accuracy of these expressions by calibrating the convolution kernels using results from previously validated physics-based models. The most impressive benefit of the MKS approach lies in the dramatic reduction of the computational cost, often by several orders of magnitude compared to numerical approaches typically employed in microstructure design problems. In various preliminary demonstrations, the MKS methodology has been successfully applied to capturing thermoelastic stress (or strain) distributions in composite RVEs [64,65,71] and multiscale structures[61], rigid-viscoplastic deformation fields in composite RVEs [72], and the evolution of the composition fields in spinodal decomposition of binary alloys [62]. Efforts are currently underway to extend the MKS to address multiscale plastic deformation of complex alloys such as Ti alloys.

On the other hand, the use of uncoupled CPFEM simulations may also result in some computational cost savings by eliminating the feedback loop between the crystal plasticity calculations and the FEM and using only the crystal plasticity after the FEM simulation is finished [73]. In this approach, the FEM exports post-simulation strain tensor and rigid-body rotations at each integration point which is then input to the crystal plasticity code to estimate texture evolution. The main drawback of this method is the lack of coupling.

In the cases where commercial FEM codes use only empirical constitutive laws (e.g., Hill yield surface), a virtual testing laboratory method [74] using a RVE approach can be used to overcome some limitations of empirical laws by fitting the yield surface to series of simulated tests. Such a numerical test protocol predicts the shape of a yield locus and then uses it to calibrate empirical constitutive models. The accuracy of this method is dependent on the ability to find best fit for the limited number of preset yield surface variables. In addition, a new yield locus needs to be generated for each new texture (starting or evolving).

Conclusions

A workflow to incorporate microstructure morphology and crystallography into modeling of TMP of titanium alloys has been summarized based on the application of data analytics for generating representative descriptors of large microstructure datasets coupled with novel techniques that may increase throughput of multiscale materials models. Representing texture using weighted orientations (based on GSH representations of ODF) enables fast data mining of orientation information and feature of interest extraction. Using the concept of a region of homogeneity defined based on the spatial distribution of the two-point correlations enables efficient insertion of a detailed quantitative microstructure description into materials models without the need to know a priori the properties of the ROH. Reducing the size of crystallographic orientation datasets

using the representative orientation distribution allows for significant increases in the speed of crystal plasticity calculations while maintaining the accuracy of predictions.

A number of options exist for solution of the crystal plasticity constitutive equations during deformation of a sample volume. Uncoupled Taylor-type simulations provide a simple methodology for estimation of final texture. For fully coupled integration of crystal plasticity into FEM simulations, the FE codes need to allow user developed subroutines that allow specification of a broad range of materials constitutive descriptions. Once again, smartly constructed databases might prove to be very practical in integrating these sophisticated materials descriptions with typically used process simulation codes.

Competing interests
The authors declare that they have no competing interests.

Authors' contributions
AAS conceived the workflow concept and created the initial draft. JBS and DPS helped with manuscript writing and analysis of exemplary datasets. SLS provided materials science guidance and expertise. SRK contributed to the overall development of the main concepts presented in this paper. All authors read and approved the final manuscript.

Acknowledgements
Support from the Air Force Research Laboratory and Air Force Office of Scientific Research is gratefully acknowledged. In particular, AAS, JBS, and DPS were partially supported by contract no. FA865009D5600 (Dr. J. Calcaterra, program manager). SRK was supported by the Air Force Office of Scientific Research, MURI contract no. FA9550-12-1-0458.

Author details
[1]Materials Resources LLC, Dayton, OH 45402, USA. [2]Air Force Research Laboratory, Materials and Manufacturing Directorate, Wright-Patterson AFB, OH 45433, USA. [3]Georgia Institute of Technology, Atlanta, GA 30332, USA.

Received: 9 May 2014 Accepted: 2 September 2014
Published online: 16 September 2014

References

1. Semiatin SL, Glavicic MG, Shevchenko SV, Ivasishin OM, Chun YB, Hwang SK (2009) Modeling and simulation of texture evolution during the thermomechanical processing of titanium alloys. In: Semiatin SL, Furrer DU (eds) ASM Handbook, Vol 22A: fundamentals of modeling for metals processing. ASM International, Materials Park, pp 536–552
2. Semiatin SL, Furrer DU (2009) Modeling of microstructure evolution during the thermomechanical processing of titanium alloys. In: Semiatin SL, Furrer DU (eds) ASM Handbook, Volume 22A: fundamentals of modeling for metals processing. ASM International, Materials Park, pp 522–535
3. Agrawal A, Deshpande PD, Cecen A, Basavarsu GP, Choudhary AN, Kalidindi SK (2014) Exploration of data science techniques to predict fatigue strength of steel from composition and processing parameters. Integr Mater Manuf Innov 3:8
4. Gibbs JW, Voorhees P (2014) Segmentation of four-dimensional, X-ray computed tomography data. Integr Mater Manuf Innov 3:6
5. Lütjering G, Williams JC (2007) Titanium. Springer, New York
6. Salem A, Glavicic M, Semiatin S (2008) A coupled EBSD/EDS method to determine the primary-and secondary-alpha textures in titanium alloys with duplex microstructures. Mater Sci Eng A 494(1):350–359
7. Kaufman L, Rousseeuw PJ (2009) Finding groups in data: an introduction to cluster analysis. John Wiley & Sons, Hoboken, NJ, USA
8. Kalidindi SR, Niezgoda SR, Salem AA (2011) Microstructure informatics using higher-order statistics and efficient data-mining protocols. JOM 63(4):34–41
9. Niezgoda SR, Kalidindi SR (2009) Applications of the phase-coded generalized hough transform to feature detection, analysis, and segmentation of digital microstructures. CMC: Comput Mater Cont 14(2):79–89
10. Bunke H, Wang PS (1997) Handbook of character recognition and document image analysis. World Scientific, New Jersey
11. Mohri M, Rostamizadeh A, Talwalkar A (2012) Foundations of machine learning. MIT Press, Cambridge, MA, USA
12. Junqué de Fortuny E, Martens D, Provost F (2013) Predictive modeling with big data: is bigger really better? J Big Data 1(4):215–226
13. Silver N (2012) The signal and the noise: Why so many predictions fail—but some don't. Penguin Press, New York
14. Salem AA, Shaffer JB (2013) Identification and quantification of microtextured regions in materials with ordered crystal structure., US Patent 13/761,612
15. Germain L, Gey N, Humbert M, Bocher P, Jahazi M (2005) Analysis of sharp microtexture heterogeneities in a bimodal IMI 834 billet. Acta Mater 53(13):3535–3543
16. Bunge H (1982) Texture analysis in materials science. Butterworths, London
17. Adams BL, Kalidindi SR, Fullwood D (2012) Microstructure sensitive design for performance optimization. Butterworth-Heinemann, Newton, MA, USA
18. Fullwood DT, Niezgoda SR, Adams BL, Kalidindi SR (2010) Microstructure sensitive design for performance optimization. Prog Mater Sci 55(6):477–562

19. Houskamp JR, Proust G, Kalidindi SR (2007) Integration of microstructure-sensitive design with finite element methods: elastic-plastic case studies in FCC polycrystals. Int J Multiscale Com 5(3–4):261–272
20. Knezevic M, Kalidindi SR (2007) Fast computation of first-order elastic-plastic closures for polycrystalline cubic-orthorhombic microstructures. Comput Mater Sci 39(3):643–648
21. Proust G, Kalidindi SR (2006) Procedures for construction of anisotropic elastic-plastic property closures for face-centered cubic polycrystals using first-order bounding relations. J Mech Phys Solids 54(8):1744–1762
22. Hill R (1963) Elastic properties of reinforced solids: some theoretical principles. J Mech Phys Solids 11(5):357–372
23. Drugan W, Willis J (1996) A micromechanics-based nonlocal constitutive equation and estimates of representative volume element size for elastic composites. J Mech Phys Solids 44(4):497–524
24. Ostoja-Starzewski M (1998) Random field models of heterogeneous materials. Int J Solids Struct 35(19):2429–2455
25. Torquato S (2002) Random heterogeneous materials. Springer-Verlag, New York
26. Niezgoda SR, Kanjarla AK, Kalidindi SR (2013) Novel microstructure quantification framework for databasing, visualization, and analysis of microstructure data. Integr Mater Manuf Innov 2:3
27. Niezgoda SR, Yabansu YC, Kalidindi SR (2011) Understanding and visualizing microstructure and microstructure variance as a stochastic process. Acta Mater 59(16):6387–6400
28. Niezgoda SR, Turner DM, Fullwood DT, Kalidindi SR (2010) Optimized structure based representative volume element sets reflecting the ensemble-averaged 2-point statistics. Acta Mater 58(13):4432–4445
29. Niezgoda SR, Fullwood DT, Kalidindi SR (2008) Delineation of the space of 2-point correlations in a composite material system. Acta Mater 56(18):5285–5292
30. Fullwood DT, Niezgoda SR, Kalidindi SR (2008) Microstructure reconstructions from 2-point statistics using phase-recovery algorithms. Acta Mater 56(5):942–948
31. Salem AA, Glavicic M, Semiatin S (2008) The effect of preheat temperature and inter-pass reheating on microstructure and texture evolution during hot rolling of Ti-6Al-4 V. Mater Sci Eng A 496(1):169–176
32. Qidwai SM, Turner DM, Niezgoda SR, Lewis AC, Geltmacher AB, Rowenhorst DJ, Kalidindi SR (2012) Estimating response of polycrystalline materials using sets of weighted statistical volume elements (WSVEs). Acta Mater 60:5284–5299
33. Wargo EA, Hanna AC, Cecen A, Kalidindi SR, Kumbur EC (2012) Selection of representative volume elements for pore-scale analysis of transport in fuel cell materials. J Power Sources 197:168–179
34. Torquato S (2009) Inverse optimization techniques for targeted self-assembly. Soft Matter 5(6):1157–1173
35. Torquato S (2010) Optimal design of heterogeneous materials. Annu Rev Mater Res 40:101–129
36. Salem A, Kalidindi SR, Doherty RD (2003) Strain hardening of titanium: role of deformation twinning. Acta Mater 51(14):4225–4237
37. Salem A, Kalidindi S, Semiatin S (2005) Strain hardening due to deformation twinning in α-titanium: constitutive relations and crystal-plasticity modeling. Acta Mater 53(12):3495–3502
38. Li H, Mason D, Bieler T, Boehlert C, Crimp M (2013) Methodology for estimating the critical resolved shear stress ratios of α-phase Ti using EBSD-based trace analysis. Acta Mater 61(20):7555–7567
39. Kalidindi SR, Bronkhorst CA, Anand L (1992) Crystallographic texture evolution in bulk deformation processing of FCC metals. J Mech Phys Solids 40(3):537–569
40. Morris PR, Semiatin SL (1979) The prediction of plastic properties of polycrystalline aggregates of BCC metals deforming by <111 > pencil glide. Texture of Crystalline Solids 3(2):113–126
41. Piehler H, Backofen W (1971) A theoretical examination of the plastic properties of bcc crystals deforming by <111 > pencil glide. Metall Trans 2(1):249–255
42. Glavicic M, Kobryn P, Goetz R, Yu K, Semiatin S (2004) Texture evolution during primary processing of production-scale vacuum arc remelted ingots of Ti–6Al–4V. In: Proc. 10th world conf. on titanium. Wiley-VCH, Weinheim, Germany, pp 1299–1306
43. Chin G, Mammel W (1967) Computer solutions of Taylor analysis for axisymmetric flow. Trans Metall Soc AIME 239(9):1400–1405
44. Burgers W (1934) On the process of transition of the cubic-body-centered modification into the hexagonal-close-packed modification of zirconium. Physica 1(7):561–586
45. Salem A, Semiatin S (2009) Anisotropy of the hot plastic deformation of Ti–6Al–4 V single-colony samples. Mater Sci Eng A 508(1):114–120
46. Kröner E (1959) Allgemeine kontinuumstheorie der versetzungen und eigenspannungen. Arch Rational Mech Anal 4(1):273–334
47. Kalidindi SR (1998) Incorporation of deformation twinning in crystal plasticity models. J Mech Phys Solids 46(2):267–290
48. Glavicic M, Goetz R, Barker D, Shen G, Furrer D, Woodfield A, Semiatin S (2008) Modeling of texture evolution during hot forging of alpha/beta titanium alloys. Metall Mater Trans A 39(4):887–896
49. Lebensohn R, Tomé C (1993) A self-consistent anisotropic approach for the simulation of plastic deformation and texture development of polycrystals: application to zirconium alloys. Acta Metall Mater 41(9):2611–2624
50. Taylor GI (1938) Plastic strain in metals. J Inst Metals 62:307–324
51. Gey N, Humbert M, Philippe MJ, Combres Y (1996) Investigation of the α- and β- texture evolution of hot rolled Ti-64 products. Mater Sci Eng A 219(1–2):80–88
52. Wu X, Kalidindi SR, Necker C, Salem AA (2007) Prediction of crystallographic texture evolution and anisotropic stress–strain curves during large plastic strains in high purity α-titanium using a Taylor-type crystal plasticity model. Acta Mater 55(2):423–432
53. Kalidindi SR, Duvvuru HK, Knezevic M (2006) Spectral calibration of crystal plasticity models. Acta Mater 54(7):1795–1804
54. Lebensohn RA, Rollett AD, Suquet P (2011) Fast Fourier transform-based modeling for the determination of micromechanical fields in polycrystals. JOM 63(3):13–18
55. Knezevic M, Al-Harbi HF, Kalidindi SR (2009) Crystal plasticity simulations using discrete Fourier transforms. Acta Mater 57(6):1777–1784
56. Al-Harbi HF, Knezevic M, Kalidindi SR (2010) Spectral approaches for the fast computation of yield surfaces and first-order plastic property closures for polycrystalline materials with cubic-triclinic textures. CMC: Comput Mater Cont 15(2):153–172

57. ABAQUS (2014) 6.13. Dassault Systèmes, Providence, RI, USA
58. Marc (2013) 2013.1. MSC Software, Newport Beach, CA, USA
59. Simufact.forming (2014) Simufact engineering GmbH. Hamburg, Germany
60. Al-Harbi HF, Kalidindi SR (2014) Crystal plasticity finite element simulations using a database of discrete Fourier transforms. Int J Plast doi:10.1016/j.ijplas.2014.04.006
61. Al-Harbi HF, Landi G, Kalidindi SR (2012) Multi-scale modeling of the elastic response of a structural component made from a composite material using the materials knowledge system. Modell Simul Mater Sci Eng 20:055001
62. Fast T, Niezgoda SR, Kalidindi SR (2011) A new framework for computationally efficient structure–structure evolution linkages to facilitate high-fidelity scale bridging in multi-scale materials models. Acta Mater 59(2):699–707
63. Kalidindi SR, Niezgoda SR, Landi G, Vachhani S, Fast T (2010) A novel framework for building materials knowledge systems. CMC: Comput Mater Cont 17(2):103–125
64. Landi G, Niezgoda SR, Kalidindi SR (2010) Multi-scale modeling of elastic response of three-dimensional voxel-based microstructure datasets using novel DFT-based knowledge systems. Acta Mater 58(7):2716–2725
65. Landi G, Kalidindi SR (2010) Thermo-elastic localization relationships for multi-phase composites. CMC: Comput Mater Cont 16(3):273–293
66. Adams BL, Kalidindi SR, Fullwood DT (2012) Microstructure sensitive design for performance optimization. Science, Elsevier
67. Kroner E (1986) Statistical modelling. In: Gittus J, Zarka J (eds) Modelling small deformations of polycrystals. Elsevier Science Publishers, London, pp 229–291
68. Kroner E (1977) Bounds for effective elastic moduli of disordered materials. J Mech Phys Solids 25(2):137–155
69. Binci M, Fullwood D, Kalidindi SR (2008) A new spectral framework for establishing localization relationships for elastic behavior of composites and their calibration to finite-element models. Acta Mater 56(10):2272–2282
70. Kalidindi SR, Binci M, Fullwood D, Adams BL (2006) Elastic properties closures using second-order homogenization theories: case studies in composites of two isotropic constituents. Acta Mater 54(11):3117–3126
71. Fast T, Kalidindi SR (2011) Formulation and calibration of higher-order elastic localization relationships using the MKS approach. Acta Mater 59(11):4595–4605
72. Kalidindi SR (2012) Computationally-efficient fully-coupled multi-scale modeling of materials phenomena using calibrated localization linkages. ISRN Materials Science doi:10.5402/2012/305692
73. Kalidindi S, Anand L (1992) An approximate procedure for predicting the evolution of crystallographic texture in bulk deformation processing of FCC metals. Int J Mech Sci 34(4):309–329
74. Kraska M, Doig M, Tikhomirov D, Raabe D, Roters F (2009) Virtual material testing for stamping simulations based on polycrystal plasticity. Comput Mater Sci 46(2):383–392

doi:10.1186/s40192-014-0024-6
Cite this article as: Salem *et al.*: **Workflow for integrating mesoscale heterogeneities in materials structure with process simulation of titanium alloys.** *Integrating Materials and Manufacturing Innovation* 2014 **3**:24.